Journal of Inorganic Biochemistry 193 (2019) 15–24

Contents lists available at ScienceDirect

Journal of Inorganic Biochemistry

journal homepage: www.elsevier.com/locate/jinorgbio

N-(6-Aminohexyl)-5-chloro-1-naphthalenesulfonamide, a centrin antagonist, inhibits Tb^{3+}/peptides-binding properties

Min Li[a,b,1], Wenlong Zhang[a,1], Binsheng Yang[a,*]

[a] Key Laboratory of Chemical Biology and Molecular Engineering of Ministry of Education, Institute of Molecular Science, Taiyuan 030006, China
[b] Department of Chemistry, Changzhi University, Changzhi 046011, China

ARTICLE INFO

Keywords:
Centrin
W-7
Inhibit
Antagonist

ABSTRACT

N-(6-Aminohexyl)-5-chloro-1-naphthalenesulfonamide (W-7), a kind of adjuvant chemotherapy, can bind to calmodulin and inhibit Ca^{2+}/calmodulin-regulated enzyme activities and cell proliferation. Similar to calmodulin, *euplotes octocarinatus* centrin (EoCen) belongs to EF-hand superfamily of calcium-binding proteins. It is associated with nucleotide excision repair (NER), cell division cycle and ciliogenesis. In the present study, the comparative interaction of W-7 with EoCen was first examined by using various spectroscopic, calorimetric methods and molecular docking. The obtain results recommend that only one W-7 molecule is identified binding to the C-terminal hydrophobic pocket of centrin that normally plays a role in anchoring targets. Methyl groups of Ala126, Met141, Ile161 and M162 of C-terminal may react with W-7 chloronaphthalene ring, other aliphatic or aromatic side-chains in a deep hydrophobic pocket of protein. Circular dichroism (CD) and fluorescence lifetime experiments reveal that W-7 triggers a conformational change of centrin. As a result, W-7 is identified to be an antagonist of centrin. It appears to inhibit the centrin-mediated activation of target proteins by blocking the hydrophobic pocket. Moreover, the complex formation leads to affinity decrease of Tb^{3+} binding to C-terminal of protein and self-assembly affected. Our present study provides the first view of centrin recognizing a naphthalene-sulfonamide derivative. It is proposed that W-7 and its analogues can serve as a useful tool for research on the participation of centrin in biological processes and cell biology-related studies.

1. Introduction

Centrin is a ubiquitous Ca^{2+}-binding protein of 168 residues. It is highly conserved member of the EF-hand superfamily. It was found throughout eukaryotes and it related to another Ca^{2+}-binding protein, calmodulin. Their common structural and functional unit is EF-hand motif. Ca^{2+} sensor EF-hand domains change conformation upon Ca^{2+} binding, from a closed to an open form [1]. Similarly with calmodulin being a calcium signal protein, a general view of how centrin works is that the binding of it to its target peptide, and low-affinity peptide binding sites becoming activated in the presence of Ca^{2+}, as in the case of Scherffelia dubia centrin [2]. Despite sharing similarity with calmodulin, centrin has mass different properties, such as self-assembly based on a disordered region of first 20 amino acids [3,4]. literature has suggested that dubia centrin forms extended filamentous structures in a calcium-dependent manner [3].

Centrin plays a fundamental role in the Ca^{2+}-dependent signaling pathways of eukaryotic cells [5–14]. Its properties and functions have been summarized in recent reviews [1]. Only about 10% of the centrins are concentrated on the microtubule organizer centers (MTOC) [15], which are structurally and functionally similar to basal bodies in ciliated and flagellated cells, the spindle pole bodies (SPB) in yeast and the centrosome in higher eukaryotes. It related to the regulation of the MTOC duplication, separation during the cell cycle, and the nuclear mRNA export machinery in yeast [16,17]. In addition, centrin distributed throughout the cell is strongly associated with the light transduction cascade in photoreceptor cells [18], the nuclear mRNA export in yeast and the ciliary voltage-gated Ca^{2+} channel in Paramecium in Tetrahymena [16,17]. Moreover, centrin may play a functional role in pre-mRNA splicing [9], regulation of neuron-specific K^{+} channel [10], breast cancer development [19] and global genome nucleotide excision repair together with xeroderma pigmentosum group C (XPC) protein, the human homologue of Rad23B (HR23B) protein [20,21]. Related to this, a variety of small organic molecules, antagonists with distinct chemical structures have been found to be the research focus inhibiting the centrin-mediated processes by direct

* Corresponding author.
E-mail address: yangbs@sxu.edu.cn (B. Yang).
[1] Contributed equally to this work.

https://doi.org/10.1016/j.jinorgbio.2019.01.002
Received 21 August 2018; Received in revised form 7 December 2018; Accepted 6 January 2019
Available online 11 January 2019
0162-0134/

interaction with centrin. To understand this broad specificity, detailed structural analyses of centrin with target proteins and small molecules are crucial. Moreover, these analyses may improve our knowledge of how centrin mediates such calcium signaling processes and how one can block a specific pathway, that would ultimately lead to therapeutic treatments for abnormal neural signal transduction.

Euplotes octocarinatus centrin (EoCen) is firstly reported by our laboratory [22] (gene register Y18899), which is obtained from *Euplotes Octocarinatu*. It contains no tryptophan and four tyrosine residues. There is a pair of EF-hand domains, namely four potential metal ion-binding sites in EoCen. N-terminal domain of EoCen is composed of first two EF-hands and involves in 101 amino acid residues. C-terminal domain of EoCen is composed of last two EF-hands and involves in 79 amino acid residues. Indeed, our previous work has suggested that N-terminal domain play a critical role in the process of EoCen self-assembly [23–25]. C-terminal domain is responsible for target peptides binding, such as melittin and XPC [8,26,27]. It has been found that metal ions (Ca^{2+} or Tb^{3+}) binds to N-terminal or C-terminal of EoCen with 2:1 stoichiometry. The binding of four metal ions to EoCen with two higher affinity sites (III and IV) located at C-terminal and two lower affinity sites (I and II) located at N-terminal [28]. The order for the metal-binding affinity of four sites in EoCen is site IV > site III > site I > site II [29,30]. Tb^{3+}, as lanthanide ion, induces larger conformation change and leads to stronger aggregation than that Ca^{2+}, even if it has similar coordination chemistry properties with Ca^{2+} [29–33]. The average affinity of Tb^{3+} to C-terminal and N-terminal is $(15.38 \pm 5.02) \times 10^6\ M^{-1}$ and $(3.08 \pm 0.18) \times 10^6\ M^{-1}$, respectively [26].

N-(6-Aminohexyl)-5-chloro-1-naphthalenesulfonamide (W-7) is frequently used to study Ca^{2+}-CaM-dependent activation of various enzymes. Acting as a putative calmodulin antagonist, W-7 binds to calmodulin and inhibits Ca^{2+}/calmodulin-regulated enzyme activities [34–36]. Its structure is shown in Fig. 1. Experiments reports that W-7 molecules bind to Ca^{2+}-CaM with a dissociation constant of 11 μM [35]. In contrast with other calmodulin antagonists such as chlorpromazine (cPZ) and trifluoperazine (TFP), W-7 penetrates the cell membrane and doesn't damage the structure of the cell membrane and then affect its fluidity [34,37]. As a kind of adjuvant chemotherapy, it can also enhance chemotherapy drug curative effect and reduce the dose of chemotherapy, thus reducing the side effects of drugs. Despite an extensive study of the reactions of calmodulin with antagonist including W-7, research about centrin with its antagonist has been never studied.

In the present study, we report the binding of W-7 to EoCen by application of multiple spectroscopic techniques, isothermal titration calorimetry (ITC), native polyacrylamide gel electrophoresis (native-PAGE) and resonance light scattering (RLS) measurements. The binding site and the orientation of W-7 in protein are clearly defined. This work is beneficial for further understanding the functions of W-7 and is analogues. The structural comparison of this structure with other published structures of centrin-ligands complexes helps to reveal the basis of diversity in molecular recognition by centrin.

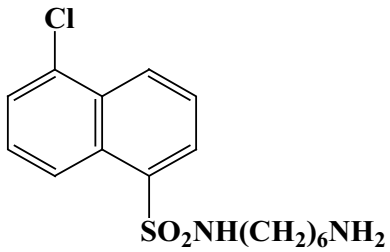

Fig. 1. The structure of W-7.

2. Experimental

2.1. Reagents

4-(2-Hydroxyethyl)-1-piperazineethanesulfonic acid (Hepes) and 2, 6-*p*-toluidinonaphthalene sulfonate (TNS) were purchased from Sigma. W-7 got from TCI. Melittin, tryptone, yeast extract, ampicillin, isopropyl-β-D-thiogalactopyranoside (IPTG), bromophenol blue and Coomassie brilliant blue R-250 were purchased from Sangon in Shanghai of China. Biochemical reagents in construction, expression and purification of proteins were obtained from Trans Gene. Tb_4O_7 with a purity of 99.9% was used. The stock solution of terbium (0.0143 M) was prepared by dissolving weighed Tb_4O_7 in concentrated hydrochloric acid, which was then standardized by complexometric titration with ethylene diamine tetraacetic acid (EDTA) using xylenol orange as the indicator in acetic acid-sodium acetate (HAc/NaAc) buffer at pH 5.5. All other chemicals were the highest purity available from local sources.

2.2. Preparation of W-7

Stock solution of W-7 was prepared in 10 mM pH 7.4 Hepes. The stock solutions were used immediately after it was ready.

2.3. Protein preparation

Using full-length gene as template, EoCen was required by polymerase chain reaction (PCR) technique. The PCR product was subcloned into a pGEX-6p-1 vector. The clone result was confirmed by DNA sequence analysis. The recombinant plasmids were transferred into *Escherichia coli* strain BL21 (DE3) and incubated in Luria Bertzani (LB) media containing 100 μg/mL ampicillin at 37 °C. When the optical density was up to 0.6–0.8 (at 600 nm), protein was induced using 0.8 mM IPTG for 3.5 h. GST fusion proteins were purified using glutathione sepharose 4FF in PBS. Isolate EoCen protein was obtained by PreScission Protease (PPase) cleavage, AKTA purifier FPLC system and passing over a HiLoadTM 16/60 SuperdexTM 200 gel filtration column. Detailed procedures were described in [25]. Protein was further identified via 15% SDS-PAGE (indicated > 99% purity). The purified proteins were conserved in 10 mM Hepes (pH 7.4) at −80 °C. Protein concentration was measured using molar extinction coefficient at 280 nm of 5600 $M^{-1}\ cm^{-1}$.

2.4. CD measurements

CD measurements were performed with an MOS 450 (BioLogic, France) spectropolarimeter. All spectra were the average of three scans with a step size of 0.2 nm and a band width of 1 nm. CD spectra were recorded between 190 and 260 nm using 1 cm path length quartz cells. All experiments were done at room temperature in Hepes (pH 7.4).

2.5. Fluorescence lifetime

Fluorescence lifetimes were collected by the time-correlated single-photon counting technique using an Edinburgh Analytical Instruments type nF-900 fluorometer. The excitation source is a flash lamp filled with hydrogen (0.4 atm) and operated at 40 kHz with approximately 6.86 kV across a 1-mm gap. Ludox HS-30 scattering solution was used to collect the instrument's response. Fluorescence decays, I(t), were measured in 10 mM Hepes, pH 7.4, at 25 °C. The excitation wavelength is selected by using monochromators at 280 nm. Emission wavelengths are 307 nm for protein and 369 nm for W-7, respectively. The fluorescence decay was analyzed using a sum of exponentials: $I(t) = \Sigma B_i \exp(-t/\tau_i)$, where B_i and τ_i are the amplitude and lifetime, respectively.

2.6. Native-PAGE analysis

Samples (EoCen, melittin and W-7) were incubated in Hepes (10 mM, pH 7.4) at 4 °C for 12 h before addition of loading buffer (1/5 volume). The loading buffer consists of 50% glycerol and 0.5% bromophenol blue. Then electrophoresis was carried out in 15% native-PAGE (acrylamide/bis-acrylamide = 29:1) containing tris-glycine buffer. Gels ran at the constant potential of 80 V. Protein was visualized in gels by stained with Coomassie brilliant blue R-250 (0.25% Coomassie brilliant blue R-250, 45% methylalcohol, 10% glacialacetic acid) using ZHGP-70I film illuminator.

2.7. Spectrofluorimetric methods

Steady fluorescence spectra were recorded on a HORIBA Scientific Fluoromax-4 spectrometer in 1 cm quartz cells at 25 °C. The excitation and emission slit width were set at 5 nm with a scan rate of 100 nm/min. The excitation wavelength was set at 280 nm for protein, 320 nm for TNS and 290 nm for Tb^{3+} in steady-state fluorescence experiments. In Tb^{3+} fluorescence experiments, a 360 nm emission filter was used. As for the affinity of W-7 towards EoCen, titration was carried out with increasing concentration of W-7 (0–2 mM) and corresponding emission spectra were recorded. Binding constant (K_a) and binding stoichiometry (n) were determined according to the formulas (1)–(6) provided in the supporting materials based on ref. [38].

2.8. Isothermal titration calorimetry assay

Isothermal titration calorimetry (ITC) experiments were performed using a MicroCal ITC200 device (MicroCal, Northampton, MA, USA) at 25 °C. The protein and W-7 were equilibrated in the same buffer containing 10 mM Hepes (pH 7.4). The instrument consists of two identical cells, one for the sample and one for the reference solution. The reference cell of the microcalorimeter was filled with ultrapure water, and both cells were maintained at the same temperature. Protein was deposited in the sample cell at 0.08 mM and it was titrated with W-7 at 0.8–2.0 mM by automatic injections of 1 μL at 25 °C. The first injection of 0.4 μL was ignored in the final data analysis. The integration of the peaks corresponding to each injection and the correction for the baseline were performed with the Origin-based software provided by the manufacturer. The data were fit to an interaction model to generate the stoichiometry (n), equilibrium binding constant (K_a) and enthalpy of complex formation (ΔH). Typically, control experiments consisting of injections of W-7 solutions into the buffer were performed to evaluate the heat of dilution. At least three replicates were performed for each experiment. The results were analyzed and calculated by the MicroCal Origin Software (MicroCal, Northampton, MA, USA).

2.9. Resonance light scattering

Solution turbidity changes were monitored by the change of fluorescence at a wavelength 370 nm of samples in 1 cm optical path quartz cells in 10 mM Hepes at pH 7.4 with a fluorescence spectrometer (F-2500, Hitachi, Japan). The slit widths of excitation and emission were both 5 nm, using the same emission and excitation wavelengths ($\Delta\lambda$ = 0 nm). The RLS signals were recorded using synchronous scanning from 250 to 600 nm.

2.10. Molecular docking

Based on experimental results, docking experiments were carried out to visualize the binding site of W-7 to EoCen. Firstly, a computational molecular model of EoCen structure was built and used as a template using the SwissModel server (DOI: https://doi.org/10.1093/nar/gku340) with default parameters [39]. The structure was obtained by using the best template, a mouse centrin 1. They share a high sequence identity of 56.16%. To generate the binary complex of W-7-EoCen, the obtained structure of EoCen by SwissModel server was chosen as a template. The binding site and the binding mode were identified by an automated public domain software package ArgusLab 4.0.1 that performs the molecular constructions, calculations, and visualizations. The possible binding conformations and orientations were analyzed by clustering methods. This dock engine was set to perform an exhaustive search for automated docking with complete ligand flexibility to elucidate the mode of interactions between W-7 and EoCen. The water molecules were removed, and the hydrogen atoms were added using the builder module of ArgusLab. The docking search was done for the whole protein without defining the target area or protein pocket. Geometry optimization was carried out with grid resolution of 0.2 Å and grid spacing of 18.62 Å × 18.44 Å × 18.80 Å. The pose with the minimal energy was taken as the optimal binding mode. To evaluate the effectiveness of the ArgusLab dock engine, docking of palmitate to βLG was done, and the resultant best pose was compared with the corresponding crystal structure of palmitate-βLG complex (PDB: 1B0O) [40]. The method was used by the binding of curcumin to CopC [41]. This validated the docking accuracy needed for further studies.

All experiments were performed in triplicate (n = 3) to ensure accuracy and reliability of the results at 25 °C.

3. Results and discussion

3.1. Conformation change

3.1.1. Circular dichroism (CD) spectroscopy

CD spectra of EoCen were recorded in the absence as well as in the presence of different concentration of W-7 (from W-7/protein ratio 0:1 to 4:1). As seen from Fig. 2, EoCen exhibits two negative CD signal at 208 nm and 222 nm (line 1), which is commonly used as quantifying α-helix of protein [42]. A drastic decrease in negative band is detected when protein complexed with W-7 at a molar ratio of 1:1, even at higher molar ratios (line 2 to line 5). In detail, the α-helix content of protein decreases by 25% than protein alone when the stoichiometric ratio of W-7 to protein is 1 (line 2). When the stoichiometric ratio of W-7 to protein is 4 (line 5), the α-helix content of protein reduce by about 50% than that protein in buffer. The results suggest that protein structure changes a lot associated with EoCen-W-7 complex formation.

3.1.2. Time-resolved fluorescence spectroscopy studies

Fluorescence lifetimes of EoCen in the presence of W-7 were

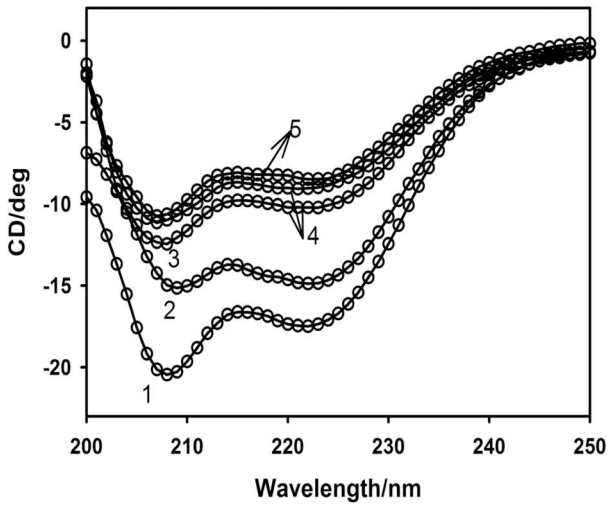

Fig. 2. CD analysis. Far-UV CD spectra of EoCen at [W-7]/[EoCen] = 0 (line 1), 1:1 (line 2), 2:1 (line 3), 3:1 (line 4), 4:1 (line 5). The protein cencentration is 6.30 μM in 10 mM pH 7.4 Hepes.

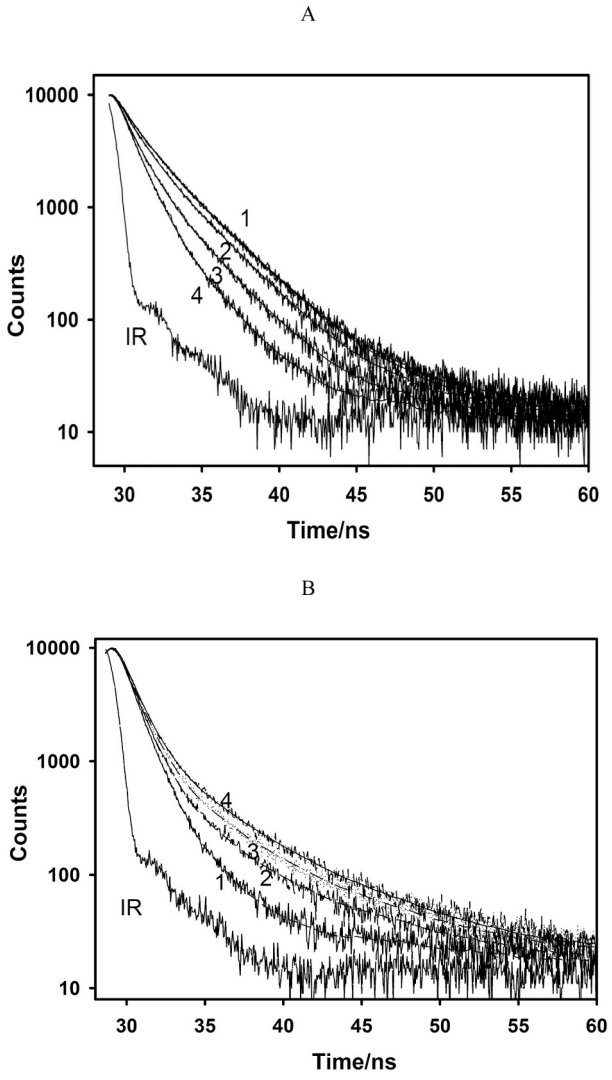

Fig. 3. Fluorescence lifetime. (a) Fluorescence lifetime decay curves of EoCen at [W-7]/[EoCen] = 0 (line 1), 1:1 (line 2), 8:1 (line 3), 25:1 (line 4), 50:1 (line 5), λem = 307 nm. (b) Fluorescence lifetime decay curves of W-7 at [EoCen]/[W-7] = 0 (line 1), 1:1 (line 2), 2:1 (line 3), 3:1 (line 4), λem = 369 nm. The protein cencentration is 6.30 μM in 10 mM pH 7.4 Hepes at 25 °C.

Table 1
The fluorescence lifetime parameters of EoCen and EoCen-W-7.

	τ_1 (%)	τ_2 (%)	$< \tau >$
EoCen	1.51 ± 0.03(45.49)	3.49 ± 0.04(54.31)	2.58
1W-7	1.45 ± 0.03(48.09)	3.46 ± 0.03(51.91)	2.49
8W-7	1.34 ± 0.02(54.60)	3.32 ± 0.03(45.40)	2.24
25W-7	1.18 ± 0.01(72.21)	3.27 ± 0.04(27.79)	1.76
50W-7	1.15 ± 0.01(90.62)	3.22 ± 0.10(9.38)	1.34

Bi, τi and $< \tau >$ are the amplitude (refer to the in parenthesis), lifetime and average lifetime, respectively.

measured and the results were presented in Fig. 3a. It can easily be seen that the lifetime of tyrosine in EoCen changes in the presence of W-7. The decays are found to be multiexponential in nature with two decay components (τ_i) and the lifetimes are listed in Table 1. For EoCen (line 1), the overall fluorescence decay leads to an average decay time ($\Sigma\tau_i B_i$) constant of 2.58 ns on the experimental conditions. The value decreases with increasing concentration of W-7 (line 2 to line 4). Remarkably, one equivalent W-7 cause minimal lifetime change of protein. Addition of

Table 2
The fluorescence lifetime parameters of W-7 and EoCen-W-7.

	τ_1 (%)	τ_2 (%)	$< \tau >$
W-7	1.05 ± 0.01(97.00%)	6.90 ± 0.39(3.00%)	1.23
1EoCen	1.08 ± 0.01(88.71%)	5.74 ± 0.10(11.29%)	1.61
2EoCen	1.10 ± 0.01(83.05%)	5.52 ± 0.07(16.95%)	1.85
3EoCen	1.11 ± 0.01(77.61%)	5.39 ± 0.05(22.39%)	2.07

Bi, τi and $< \tau >$ are the amplitude (refer to the in parenthesis), lifetime and average lifetime, respectively.

abundant W-7 into EoCen ([W-7]/[EoCen] = 25) leads to the average decay time constant of 1.76 ns. The faster fluorescence decay is probably a consequence of that the binding of protein with W-7 changes the microenvironment of tyrosine [43]. Those observations suggest strongly that the interaction between W-7 and EoCen has a comparatively effect on the conformation of EoCen, which matches the CD results.

Fig. S1 shows the fluorescence decays of W-7 in DMF or H_2O, and Table S1 indicates the average lifetime of W-7 in different solutions obtained according to Fig. S1. As seen in Fig. S1, the more hydrophobic the environment around W-7 is, the greater the lifetime of W-7 is.

Fluorescence lifetimes of W-7 in the absence and presence of EoCen were measured, and the results were presented in Fig. 3b and Table 2. The average lifetime of W-7 in H_2O is 1.23 ns on the experimental conditions. The value increases upon addition the increasing concentration of EoCen. It reveals the formation of EoCen-W-7 complex. And, the slower fluorescence decay is because of the binding of W-7 with hydrophobic pocket of protein.

3.1.3. Hydrophobic cavity change monitored by TNS

TNS is widely used as a biological probe to detect the exposed hydrophobic surface based on hydrophobic interaction between it and apolarity regions of protein structure [44].

EoCen-W7 displays an emission maximum at 369 nm (line 1). The emission intensity of TNS is fairly small in Hepes (10 mM, pH 7.4) with an emission maximum at 506 nm (line 2 in Fig. S2). TNS has a high affinity for EoCen, the TNS-EoCen solution displays a large relative fluorescence intensity together with a blue shift of 71 nm compared to that in buffer as a result of the attachment of TNS to the protein (435 nm) (line 3). This is in line with our previous reports [44]. Strikingly, a considerable decrease in the fluorescence intensity at 369 nm is found, accompanied by the enhancement in the fluorescence intensity at 435 nm upon addition of TNS to EoCen-W7 solution. The changes owe to that TNS occupies hydrophobic core of protein and EoCen-W-7 complex is disassociation. The results verify that W-7 binds to the hydrophobic pocket of protein. It is in line with the fluorescence lifetime outcomes.

3.1.4. Native-page assay

EoCen was incubated with the melittin and W-7 at 4 °C over night, the sample was analyzed by native PAGE. As shown in Fig. 4. EoCen alone appears one band (lane 1). A new band produces and EoCen-melittin complex forms upon addition melittin into EoCen (lane 2), which is in keeping with our previous results [27]. Melittin forms complex with the C-terminal of EoCen while the N-terminal is not involved in complex formation [27]. The complex completely disappears when EoCen, W-7 and melittin co-exist at the same time (lane 3). It reveals that the formation of melittin-EoCen complex suffers from inhibition in the presence of W-7. It implies that the binding site of W-7 in protein may locate at C-terminal of EoCen.

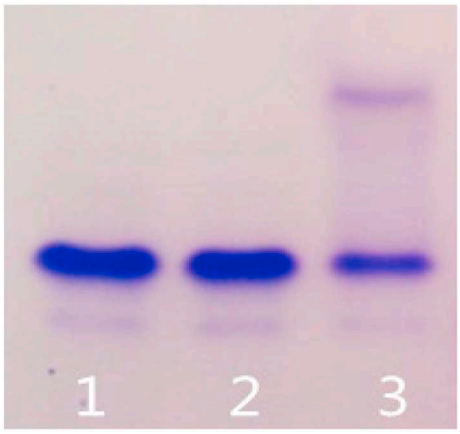

Fig. 4. Binding of W-7 to C-EoCen. Native-PAGE of EoCen in the absence or presence of melittin and W-7 after 12 h in-cubation at 4 °C. lane 1: EoCen, lane 2: EoCen + W-7 + melittin, lane 3: EoCen + melittin. The concentrations of EoCen, melittin, W-7 were 10 μM, 10 μM and 0.5 mM, respectively.

3.2. Formation of EoCen-W-7 complex

3.2.1. Fluorescence spectra

To investigate the interaction between EoCen and W-7, the steady state fluorescence spectroscopy was observed. EoCen lacks tryptophan residues and contains four tyrosine residues, among which three locate at N-terminal (Tyr46, 72, 79) and one at C-terminal (Tyr168). Therefore, changes in spectra attribute to the micro-environment change of tyrosine residues.

The maximum emission wavelength of EoCen is observed at 307 nm (λex = 280 nm) in Hepes, whereas the fluorescence emission of W-7 appears at 372 nm (Fig. 5a). Adding one equivalent of W-7 to EoCen results in about 20% decrease in intensity of protein at 307, accompanied by a blue-shift (from 372 to 369 nm) of the emission maximum of W-7. It indicates that EoCen-W-7 complex forms and W-7 may transfer from aqueous environment to a more hydrophobic core created by the C-terminal domain of EoCen.

To obtain the affinity of W-7 to EoCen, EoCen solution was titrated with W-7 progressively in 10 mM pH 7.4 Hepes. The fluorescence titration spectra (inset of Fig. 5b) show a gradual decrease in the intensity at 307 nm and an isosbestic fluorescence point. Titration curves were plotted from the decreased value of the intensity at 307 nm vs. the ratio of W-7 to EoCen. As shown in Fig. 5b, the fluorescence intensity decreases with an increase in the ratio of W-7 to EoCen and reaches a plateau at [W-7]/[EoCen] = 1.0. It indicates that the complex is formed with a 1:1 stoichiometric ratio under the condition. Analysis of the titration curve according to Eqs. (1)–(6) in supporting materials shows that W-7 binds EoCen with an apparent association constant (K_a) of $(3.73 \pm 0.14) \times 10^3\,M^{-1}$ with a stoichiometric ratio of about 1, the parameters were listed in Table 3.

3.2.2. ITC assay

The thermodynamics of the complex formation was further analyzed by ITC (Fig. 5c) and all parameters were listed in Table 3. The experimental data could be best fit into a one-site binding model with an equilibrium association constant $(4.89 \pm 0.04) \times 10^3\,M^{-1}$. The molar ratio approaches to 1. The results are closely to that obtained from the spectrofluorimetric titrations. The formation of W-7-EoCen complexation is an exothermic reaction accompanied by positive ΔS values. A positive S value is frequently taken as a typical evidence for hydrophobic interaction [45]. Therefore, the positive ΔS and ΔH values are thermodynamically characteristic for the specific type of hydrophobic interaction between W-7 and EoCen. Furthermore, it is found that the major contribution to ΔG arises from the ΔS rather than from ΔH, so we can say that, the binding process is entropy driven.

3.2.3. Förster's resonance energy transfer (FRET) analysis

According to the Forster's non-radiation energy transfer theory [46], the possibility of energy transfer occurs only when the UV–absorption spectra of acceptor molecules (W-7) and the fluorescence emission spectra of the donor molecule (EoCen) possess enough overlie and the distance between acceptor and donor is not more than 7 nm [47]. In order to calculate the possibility of energy transfer between donor to acceptor using the FRET method, the single fluorescence spectra of protein and the absorption spectrum of W-7 were plotted (Fig. 6). According to FRET theory, efficiency of energy transfer (E), spectral overlap (J), distance between the donor and acceptor (r), and Förster's distance (R_0) were derived from the overlaid spectra and the value of energy transfer between W-7 and protein were calculated from the Eqs. (7)–(9) in supporting materials. J can be evaluated by integrating the spectra in Fig. 6 for λ = 290–340 nm of $3.62 \times 10^{-15}\,cm^{-3}\,M$. In this case, R_0 was calculated at 2.16 nm from Eq. (8), using $K_2 = 2/3$, n = 1.336 and Φ = 0.14 [48], the energy transfer effect E = 0.20, and the distance between the tyrosine residue and the bound W-7 was obtained $r = 2.72$ nm. Because W-7 binds to C-terminal merely containing one tyrosine (Tyr168), energy transfer happens between aromatic ring of Tyr168 and naphthalene ring of W-7. The donor to acceptor distance r was < 7 nm, and nonradiative energy transfer occurred with high probability. In the present study, $0.5R_0 < r < 1.5R_0$ is observed, which reveals the presence of the static quenching mechanism to a large extent, namely a EoCen-W-7 complex forms.

3.2.4. Visualization of the binding site: Docking studies

On the basis of the experimental data, computational docking studies were performed to understand the binding site location and binding mode of W-7 to EoCen. The representative build derived from the best pose with the minimal binding energy of $-10.22\,kcal\,mol^{-1}$ is shown in Fig. 7. The distance between W-7 and Tyr168 of EoCen was 1.41 nm (Fig. 7), which approaches to the spectroscopic data 2.16 nm.

In one word, W-7 can form 1:1 complex with EoCen. The complex formation mainly depends on the hydrophobic core formed by C-terminal. The distance between Tyr168 residue and the bound W-7 is 1.41 nm. W-7 chloronaphthalene ring may interact with methyl groups of Ala126, Met141, Ile161 and M162 of EoCen. Other aliphatic or aromatic side-chains of W-7 are in a deep hydrophobic pocket of protein.

3.3. Inhibitory effect of W-7 on metal ions binding properties of centrin

Based on previous reports, the affinity order for Tb^{3+}-binding of four sites in EoCen acquired by spectroscopic and electrochemical methods is site IV > site III > site I > site II [29,30]. C-terminal domain of EoCen has a lower tendency to aggregate and it is a key region for interaction with target protein. And the N-terminal domain has a greater contribution to self-assembly. Herein, the effects of W-7 on Tb^{3+}-binding capacity of EoCen were monitored.

3.3.1. Resonance light scattering assay

Firstly, the self-assembly behaviors of EoCen induced by Tb^{3+} in the absence or presence of W-7 were investigated by RLS experiments. The addition of Tb^{3+} leads to RLS signal increasing significantly (Fig. 8a). It implies that EoCen forms large fractal structures, exhibiting strong scattering signal. The titration curve obtained for Tb^{3+} to EoCen shows two slopes (Fig. 8b). When a solution of EoCen was added into the first 2 equivalents Tb^{3+}, RLS increases slightly, and with combining the additional 2 equivalents Tb^{3+}, RLS enhances remarkably (Fig. 8b, line 1). The slope that of the last two equivalents of Tb^{3+} addition is larger than that of the first two equivalents of Tb^{3+} addition, indicating that the sensitivity of the last two equimolar bound Tb^{3+} is higher than that of the first two. Considering that EoCen has two tight Tb^{3+} binding sites (III/IV site) in the C-terminal domain and two weak binding sites (I/II site) in the N-terminal domain [26], the results above suggest that

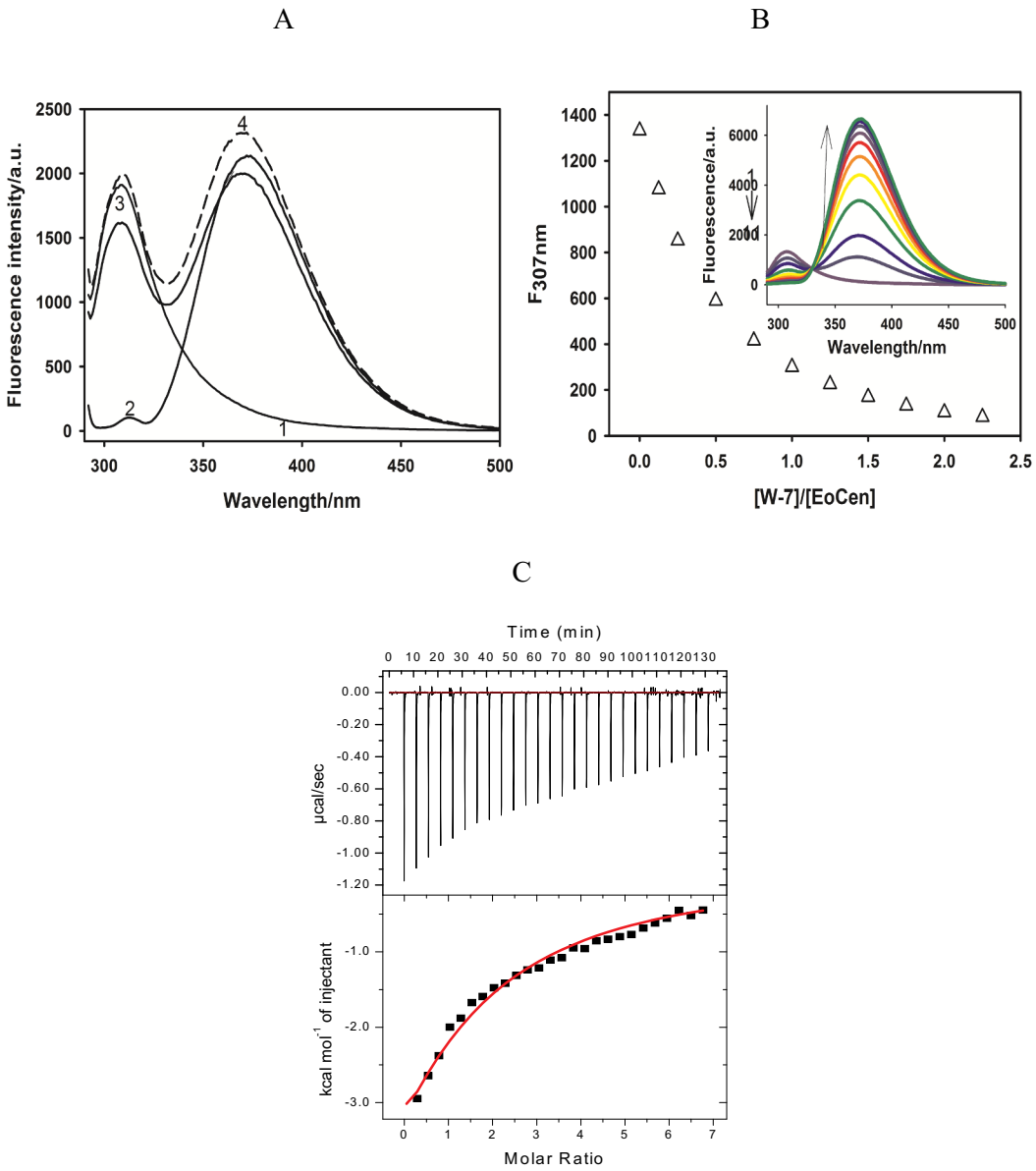

Fig. 5. W-7 binds to EoCen. (a) The fluorescence spectra of EoCen (line 1), W-7 (line 2), the mixture solution of EoCen and W-7 (line 3), the calculated sum spectra of W-7 and EoCen (line 4). The concentration of EoCen and W-7 are 6.30 μM in 10 mM pH 7.4 Hepes. (b) Plot of fluorescence intensities of protein at 307 nm as a function of [W-7]/[EoCen]. Inset: Fluorescence spectra of EoCen titrated with increasing concentration of W-7, the ratio of W-7 to EoCen is 0, 1, 2, 4, 6, 8, 10, 12, 14, 16, and 18 corresponding to line 1-11 respectively in 10 mM pH 7.4 Hepes buffer at 25 °C. The cencentration of EoCen is 6.30 μM. (c) Calorimetric titration of W-7 to EoCen at 25 °C. The solid lines represent the best fit for one set of sites model.

the binding of Tb^{3+} to EoCen is a sequential process. The first two equivalents Tb^{3+} binds to the C-terminal domain causing little polymerization. And, the last two equivalents Tb^{3+} binds to the N-terminal domain, favor the polymerization of EoCen. It is consistent with previous study [26,28]. If the RLS signal of Tb^{3+}-EoCen aggregates in the absence of W-7 is set as 100% intensity, contributions of N-terminal and C-terminal to aggregation on the conditions are 80% and 20%, respectively.

As for EoCen-W-7 solution with a ratio of 1:1, similar results are observed when the solution was added into 4 equivalents Tb^{3+} (line 2). However, when the ratio of W-7 to EoCen increase ([W-7]: [EoCen] = 8:1, 25:1, 50:1) (line 3–5), a remarkable change is exhibited

Table 3
Summary of the thermodynamic parameters for W-7 binding to EoCen determined by spectrofluorimetric methods and ITC at 25 °C.

	K (error) (10^3)	N (error)	$\triangle H^b$ (error) (kJ·mol^{-1})	ΔS^b (J·mol^{-1}·deg^{-1})	$\triangle G^b$ (kJ·mol^{-1})
W-7 + EoCen	3.73 (0.14)[a] 4.89 (0.04)[b]	1.01 (0.03)[a] 1.02 (0.02)[b]	8.5 (0.15)	46.7	−5.44

[a] Data from spectrofluorimetric titrations.
[b] Data from ITC titrations.

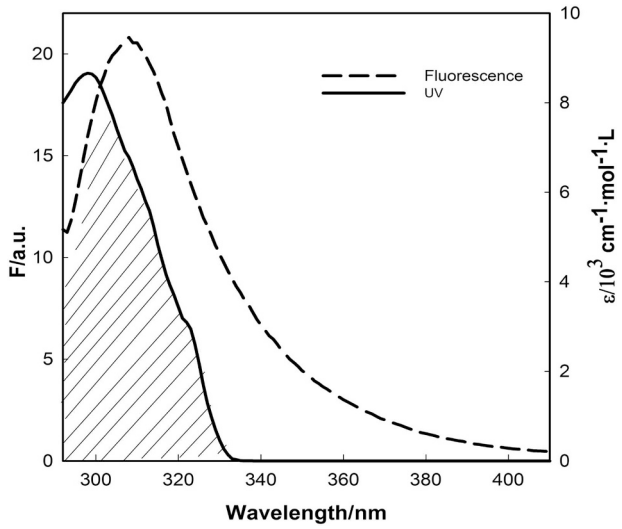

Fig. 6. The overlap of EoCen fluorescence spectrum and W-7 absorption spectrum.

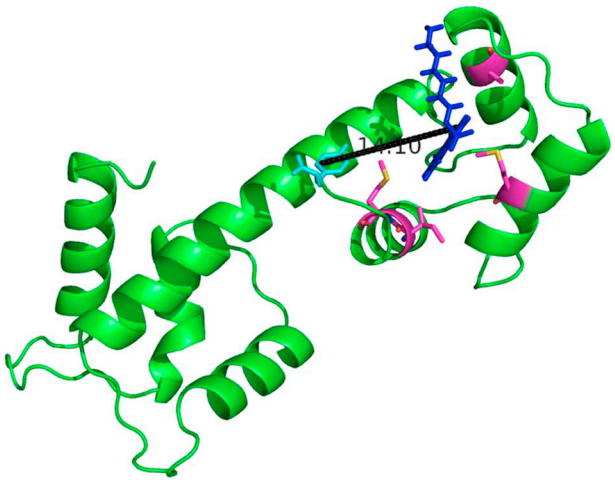

Fig. 7. Molecular docking studies. Cartoon ribbon model structure of EoCen modeled by SwissModel showing the distance (black line) between Tyr168 (cyan) and W-7. The hydrophobic amino acids in EoCen (Ala126, Met141, Ile161 and Met162) playing key roles in W-7 binding to protein show magenta sticks.

for Tb^{3+} induced aggregation process. Despite two slopes appear upon Tb^{3+} adding, the first slopes change longer with more W-7 existing. Moreover, it is found that the RLS intensity of Tb^{3+}-EoCen aggregates decrease slightly in the presence of W-7.

With regard to EoCen-W-7 with a ratio of 1:8, the RLS intensity does not change until 5 equivalents Tb^{3+} was added (line 3). When the ratio of Tb^{3+} to EoCen ranges from 3.0 to 5.0, the shape of the titration curve is identical to that of the last two equivalents Tb^{3+} binding to EoCen alone. It suggests a high similarity for Tb^{3+}-binding properties between N-terminal domain of EoCen alone or as a part of EoCen-W-7. However, when the ratio of Tb^{3+} to EoCen ranges from 0 to 3.0, the shapes of the titration curve obtained for Tb^{3+} to EoCen are different in the presence and absence of W-7. Remarkably, W-7 changes the binding capacity of Tb^{3+} to C-terminal. In addition, the RLS intensity of EoCen induced by Tb^{3+} in the presence of W-7 ([W-7]:[EoCen] = 8:1) decreases mildly, about 93% of that EoCen alone. The contributions of N-terminal and C-terminal to aggregation are 79% and 21%, respectively.

When the ratio of W-7 to EoCen reaches to 25 (line 4) and 50 (line 5), protein needs 7 and 9 equivalents Tb^{3+}, respectively. The shapes of titration curve that the last two equivalents Tb^{3+} addition in the presence of W-7 are analogous to that of the last two equivalents Tb^{3+} binding to EoCen alone. In other words, the presence of W-7 has almost no effect on the Tb^{3+}-binding capacity to N-terminal. Nevertheless, more Tb^{3+} is needed for C-terminal binding. The ratio of Tb^{3+} to the C-terminal of EoCen ranges from 2.0 to 5.0 or 7.0 in the presence of 25 or 50 equivalents W-7, respectively. Namely, the presence of W-7 causes the binding capacity of Tb^{3+} to C-terminal decrease. Moreover, the RLS intensities of EoCen-Tb^{3+} decrease by 12% when concentration ratio of W-7 to EoCen is 25. At the same time, the contribution of N-terminal to aggregation reduces to 71% and C-terminal is 29% on the condition. When the ratio of W-7 to EoCen is up to 50, the RLS intensity decreases by 24%, the contribution of C-terminal to aggregation increasing to 53%.

In order to further evaluate the effect of W-7 on the affinity of Tb^{3+} to C-terminal, the first slopes of Tb^{3+} binding were closely observation (Fig. S3). The affinities were estimated according to the formulas (1)–(6) provided in supporting materials and results are listed in Table 4. Obviously, the affinities (Table 4) reduce gradually when the ratio of W-7 to protein ranges from 0 to 50.

Overall, W-7 binding to EoCen has a significant influence on the affinity of Tb^{3+} to C-terminal. Besides, the aggregation of protein suffers from some impacts, the contribution of N-terminal to aggregation decreasing and C-terminal increasing.

3.3.2. Tb^{3+} probe

Soon afterwards, Tb^{3+} was further used as a convenient probe to monitor the effects of W-7 on the binding ability of it to protein with or without W-7.

Four characteristic peaks for Tb^{3+} at 490, 545, 580, and 620 nm are observed upon Tb^{3+} adding to EoCen due to non-radiative energy transfer from the aromatic residues to the bound Tb^{3+} (Fig. 8c). Titration curves were obtained from the sensitized Tb^{3+} emission at 545 nm vs. the ratio of Tb^{3+} to protein. As clearly seen in Fig. 8d, as for EoCen, there are four metal ion binding sites. The fluorescence intensity of the Tb^{3+} emission increases gradually in a [Tb^{3+}]/[EoCen] ratio range from 0 to 2. It attributes to that Tb^{3+} binds to the strong binding sites with low sensitization corresponding to C-terminal. The fluorescence intensity increases dramatically at a [Tb^{3+}]/[EoCen] ratio in the range from 2 to 4. This reveals that Tb^{3+} binds to the weak binding sites with high sensitization corresponding to N-terminal. It is consistent with the RLS result, binding occurs initially at the two high-affinity sites (sites III and IV in the C-terminal domain) followed by at the two low-affinity sites (sites I and II in the N-terminal domain).

A significant change is monitored for sensitized Tb^{3+} emission of EoCen in the presence of W-7. The more W-7 is, the weaker the strength of sensitized Tb^{3+} emission is. If the sensitized Tb^{3+} emission intensity of four Tb^{3+} binding to EoCen in the absence of W-7 is set as 100% intensity, W-7-EoCen solutions with a ratio of 1:1 (line 2) or 8:1 (line 3) lead to sensitized Tb^{3+} emission intensity decreases by 32% or 76%, respectively. Excessive W-7 ([W-7]:[EoCen] = 25:1, 50:1) (line 4, 5) results in completely disable for Tb^{3+} sensitization. Apparently, the binding of W-7 to protein has a vivid impact on the Tb^{3+} sensitization properties of EoCen. Even though W-7 binding has almost no impact on the binding capacity of Tb^{3+} to N-terminal showed by RLS experiments, Tb^{3+} sensitization is completely different. It may be due to that conformation change of EoCen induced by W-7 binding, especially that of N-terminal, which goes against non-radiative energy transfer occurring. It is in accordance with CD spectra and lifetime results.

Taken together, our vitro studies support the notion that Tb^{3+} affinity to C-terminal can be dramatically influenced by W-7 binding. Conformation of protein changes a lot upon W-7 binding. Moreover, W-7 binding has certain effect on the aggregation properties of protein. Contributions of N-terminal to self-assembly decreases, C-terminal increasing. Namely, W-7 binding to C-terminal has a long-range effect on the properties of N-terminal.

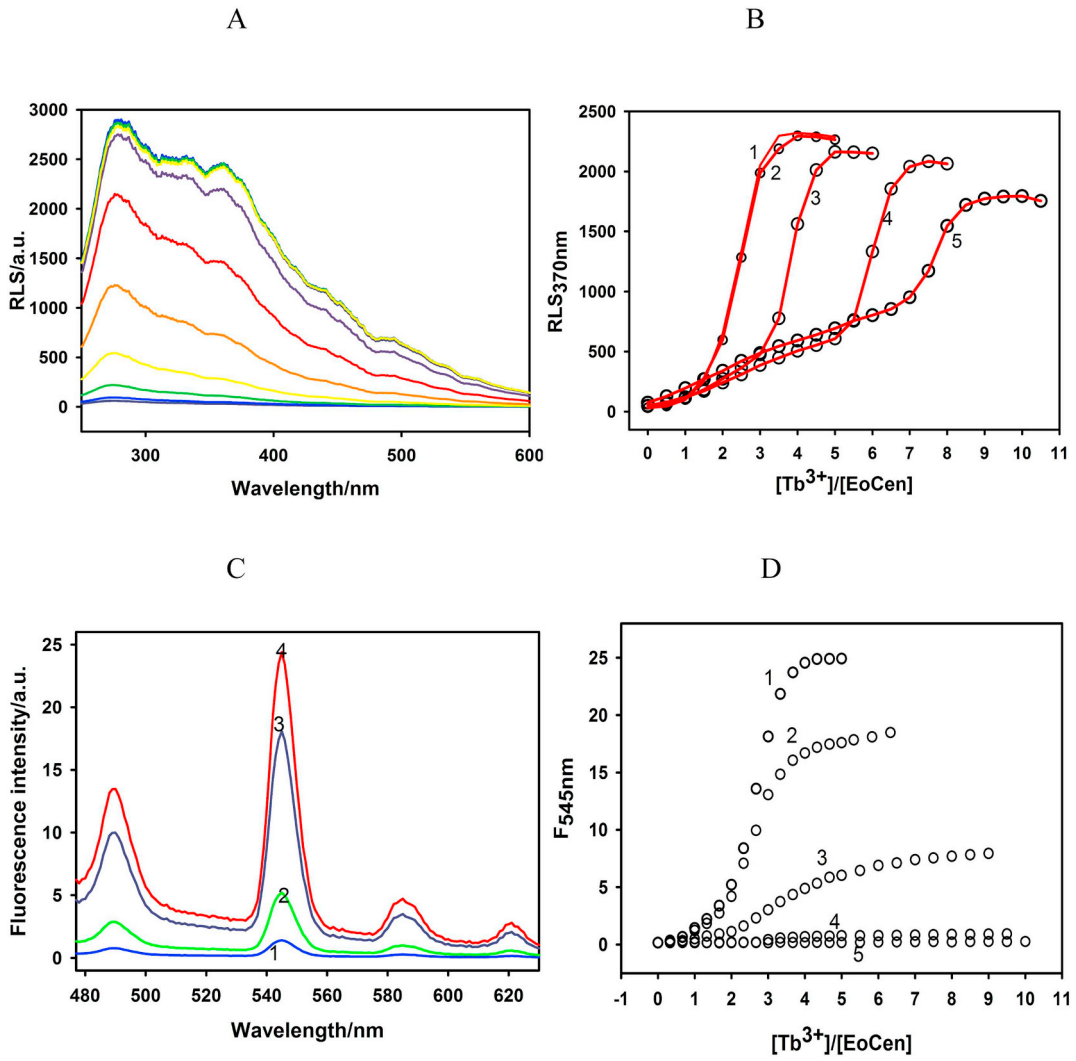

Fig. 8. Modulation of W-7 on the T^{b3+}-binding to EoCen. (a) Resonance light scattering spectra of EoCen with addition of Tb^{3+} in 10 mM pH 7.4 Hepes. (b) Resonance light scattering intensity of EoCen in the absence or presence of W-7 at 370 nm as a function of $[Tb^{3+}]$/[EoCen], the ratio of W-7 to EoCen is 0 (line 1), 1 (ling 2), 8 (line 3), 25 (line 4). (c) Tyrosine-sensitized Tb^{3+} fluorescence spectra of EoCen. The concentration ratio of W-7 to EoCen is 1, 2, 3, and 4 corresponding to line 1, line 2, line 3, and line 4, respectively. (d) Fluorescence intensity of Tb^{3+} at 545 nm as a function of the concentrations of Tb^{3+}, the ratio of W-7 to EoCen is 0 (line 1), 1 (ling 2), 8 (line 3), 25 (line 4). The cencentration of EoCen is 6.30 μM.

Table 4
Summary of constants for Tb^{3+} binding to EoCen in the absence or presence of W-7 determined by spectrofluorimetric methods at 25 °C. K is the affinity of Tb^{3+} to C-terminal in the absence or presence of W-7.

[W-7]/[EoCen]	K (error) (10^4)	RLS intensity	Aggregation contribution	
			C-terminal	N-terminal
0 (EoCen alone)	435,000	1	20%	80%
1	435,000	1	20%	80%
8	326	0.93	21%	79%
25	58.7	0.88	29%	71%
50	4.10	0.76	53%	47%

Based on obtained experimental results, a mechanistic model interpreting the interaction of W-7 and EoCen under physiological condition is proposed (Fig. 9).

In the absence of W-7, EoCen shows high affinity to melittin (K_{PT}) or Tb^{3+} (K_{PM}). Upon formation of centrin-melittin complex, melittin undergoes a conformation change from random coil state to α-helix form [27]. Similarly to the complex of *Chlamydomonas reinhardtii* centrin with melittin, C-terminal of EoCen serves as the key part determined the interaction between centrin with targets. Previous research has demonstrated that target binding of XPC to C-terminal decreases the average affinity of Tb^{3+} to protein ($K_{PM} > K_{PM}''$). In detail, it largely weakens the binding of Tb^{3+} to the N-terminal domain in EoCen and slightly enhances the affinity of the C-terminal domain of EoCen towards Tb^{3+} [26]. Self-assembly of EoCen induced by Tb^{3+} binding is inhibited in the presence of XPC [26]. Melittin also displays similar results (data not shown) (lower lane in Fig. 9).

With regard to the coordination with Tb^{3+} of EoCen, protein can bind four equivalents Tb^{3+}. High affinity sites locate at C-terminal ($(15.38 \pm 5.02) \times 10^6\,M^{-1}$) and low affinity sites locate N-terminal ($(3.08 \pm 0.18) \times 10^6\,M^{-1}$) [26]. Tb^{3+} binding render protein form aggregates (middle lane in Fig. 9).

W-7 has a good affinity to EoCen (K_{PW}). It may insert into the hydrophobic pore made up by four helix of C-terminal domain, among which, methyl groups of Ala126, Met141, Ile161 and M162 may react with W-7 chloronaphthalene ring. Other aliphatic or aromatic side-chains of W-7 are in a deep hydrophobic core of protein. The site is responsible for centrin binding to target peptides such as melittin and XPC. This competitive binding at the same site between W-7 and targets suggests the mechanism by which W-7 inhibits centrin to activate the

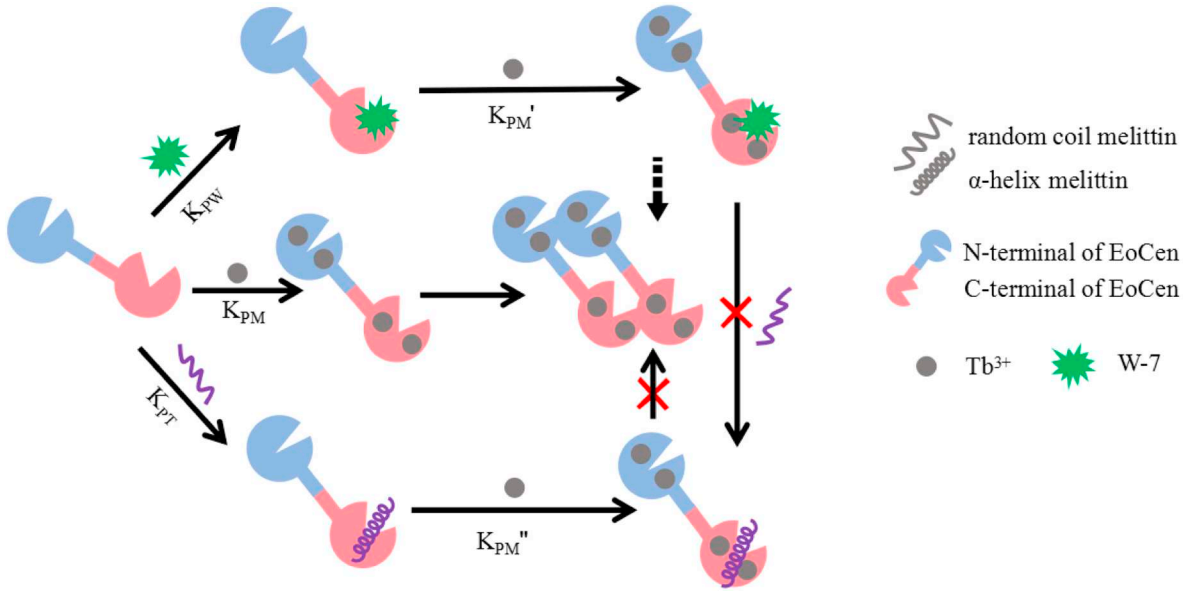

Fig. 9. Proposed model for modulation effect of W-7 on the properties of centrin according to the data available. KPW represents affinity of W-7 to EoCen. KPM and KPT represents affinities of EoCen to Tb^{3+} or targets, respectively. K_{PM}' and K_{PM}'' are average affinity of Tb^{3+} to W-7-EoCen or EoCen-targets, respectively.

targets (upper lane in Fig. 9).

Comparison with the previously reported structures of calmodulin complexed with W-7, the orientation of the W-7 naphthalene ring in the C-terminal pocket of centrin is slightly different (Fig. 9). Here, W-7 chloronaphthalene ring is surrounded by the four hydrophobic amino acids (Ala126, Met141, Ile161 and M162). In calmodulin, the W-7 chloronaphthalene ring adopts a face-to-face binding mode to four methionine methyl groups (1mux.pdb), which might be more conducive to reaction. Therefore, W-7 has a higher affinity to calmodulin. Besides, the orientation of the W-7 naphthalene ring in the C-terminal pocket of centrin is completely different from that aromatic ring of targets in the C-terminal pocket of centrin. These comparative structural analyses demonstrate that the hydrophobic pocket of centrin can accommodate a variety of bulky aromatic rings by vary conformation. This not only provides a plausible structural basis for the diversity in centrin-mediated molecular recognition, but also understanding the properties difference of centrin and calmodulin. Furthermore, this structural difference can explain why these drugs display different anticalmodulin/anticentrin activities.

The coordination with EoCen of W-7 is completely disadvantageous to Tb^{3+}-binding proceeding. In detail, W-7 has no almost impact on the affinity of Tb^{3+} towards the N-terminal domain of EoCen, whereas dramatically decreases the affinity of Tb^{3+} to the C-terminal domain in EoCen by about 10^5 times ([W-7]:[EoCen] = 25:1). Namely, protein shows a reduced average affinity to Tb^{3+} in the presence of W-7 ($K_{PM} > K_{PM}'$). These mean that the binding of W-7 to EoCen modulates the binding properties of Tb^{3+} to protein, especially C-terminal. Furthermore, we found that the excess existence of W-7 leads to aggregation extent of protein decrease, and that cooperatively induces decreasing contributions of N-terminal to aggregation, as compared to protein alone. Conformation change induced by W-7 binding goes against non-radiative energy transfer happening. Our approach provides information that the basic structural and functional unit of several EF-hand proteins is a pair of EF-hand motifs that form a stable domain, whose activity is often linked to an inter-site cooperative effect.

Being a calcium signal protein, a general view of how centrin works is that the binding of calcium facilitates target peptide recognition by the protein, as in the case of Scherffelia dubia Centrin [2]. So far, at least five proteins (XPC, Sfi1, Sac3, POC5, Transducin β) have been shown to bind centrin. Thus, centrin is involved in several cellular processes via its targets: DNA repair via XPC, spindle pole body duplication via Sfi1, RNA export via Sac3 and transduction via transducin β [49]. Besides, self-assembly of protein in the presence of metal ions plays a causative role in fiber contraction associated with the cell division cycle and ciliogenesis. Herein, a naphthalene-sulfonamide derivative acting as a centrin inhibitor was first identified. The studies provide important insight into how centrin mediates such calcium signaling processes and a plausible structural basis for understanding the diversity and differences in centrin-mediated molecular recognition. More importantly, these significant outcomes of this work towards chemical-biological interaction provide a magnificent knowledge in relation to new drug designing.

4. Conclusions

In summary, the interaction between centrin complexed with W-7 was first characterization by multi-spectroscopy methods and calorimetry method. The binding site and the orientation of W-7 in protein were defined. Only one W-7 molecule was identified binding to the C-terminal of centrin. The drug makes extensive contacts with hydrophobic residues in the C-terminal domain, among which, Ala126, Met141, Ile161 and Met162 play important roles in binding process. As a result, the binding mode is sufficient to lead to deactivation of its targets and cause the conformation changes in centrin. Furthermore, it results in Tb^{3+}-binding capacity of C-terminal decrease as well as aggregation decreasing. Consequently, W-7 works as an inhibitor of centrin. The findings may provide new insights into potent roles of W-7 and its derivatives in cell biology research of centrin. Additionally, it has guiding significance for the research of new drugs.

Abbreviations

W-7	N-(6-Aminohexyl)-5-chloro-1-naphthalenesulfonamide
EoCen	*Euplotes octocarinatus* centrin
NER	nucleotide excision repair
CD	Circular dichroism
MTOC	microtubule organizer centers
SPB	spindle pole bodies
XPC	xeroderma pigmentosum group C protein
HR23B	human homologue of Rad23B protein
ITC	isothermal titration calorimetry
native-PAGE	native polyacrylamide gel electrophoresis

RLS	resonance light scattering
Hepes	4-(2-Hydroxyethyl)-1-piperazineethanesulfonic acid
TNS	2, 6-p-toluidinonaphthalene sulfonate
IPTG	isopropyl-β-D-thiogalactopyranoside
EDTA	ethylene diamine tetraacetic acid
PCR	polymerase chain reaction
PPase	PreScission Protease
FRET	Förster's resonance energy transfer

Acknowledgments

This work was supported by the National Natural Science Foundation of China [grant numbers No. 21571117, No. 20901048 and No. 20771068], the PhD Programs Foundation of the Ministry of Education of China (grant number 20131401110011). We thank T. Zhang of scientific instrument center of Shanxi University for her excellent technical assistance in ITC.

Appendix A. Supplementary data

Supplementary data to this article can be found online at https://doi.org/10.1016/j.jinorgbio.2019.01.002.

References

[1] W.J. Chazin, Acc. Chem. Res. 44 (2011) 171–179.
[2] L. Radu, I. Durussel, L. Assairi, Y. Blouquit, S. Miron, J.A. Cox, C.T. Craescu, Biochemistry 49 (2010) 4383–4394.
[3] A. Yang, S. Miron, P. Duchambon, L. Assairi, Y. Blouquit, C.T. Craescu, Biochemistry 45 (2006) 880–889.
[4] T.J. Dantas, O.M. Daly, C.G. Morrison, Cell. Mol. Life Sci. 69 (2012) 2979–2997.
[5] Y.Q. Zhao, X.F. Chu, B.S. Yang, Bioelectrochemistry 117 (2017) 15–22.
[6] R.L. Wright, J.L. Salisbury, J.W. Jarvik, J. Cell Biol. 101 (1985) 1903–1912.
[7] G.I. Mcfadden, D. Schulze, B. Surek, J.L. Salisbury, M. Melkonian, J. Cell Biol. 105 (1987) 903–912.
[8] E.X. Shi, W.L. Zhang, Y.Q. Zhao, B.S. Yang, RSC Adv. 7 (2017) 27139–27149.
[9] A.D. Casas, W.J. Chazin, B. Pastrana-Ríos, Biophys. J. 112 (2017) 2529–2539.
[10] P.H. Hsu, Y.C. Chiu, T.F. Lin, C.J. Jeng, FEBS Open Bio 6 (2016) 349–357.
[11] J.L. Shi, Y. Zhao, T. Vonderfecht, M. Winey, M.W. Klymkowsky, Sci. Rep. 5 (2015) 10283.
[12] J. Martinez-Sanz, L. Assairi, Biochim. Biophys. Acta 1864 (2016) 319–330.
[13] W.L. Zhang, E.X. Shi, Y.Q. Zhao, B.S. Yang, J. Inorg. Biochem. 180 (2018) 15–25.
[14] W.L. Zhang, E.X. Shi, Y.Q. Zhao, B.S. Yang, RSC Adv. 7 (2017) 51773–51788.
[15] A. Paoletti, M. Moudjou, M. Paintrand, J.L. Salisbury, M. Bornens, J. Cell Sci. 109 (1996) 3089–3102.
[16] T. Fischer, S. Rodriguez-Navarro, G. Pereira, A. Racz, E. Schiebel, E. Hurt, Nat. Cell Biol. 6 (2004) 840–848.
[17] K.K. Resendes, B.A. Rasala, A.D.J. Forbes, Mol. Cell. Biol. 28 (2008) 1755–1769.
[18] A. Giessl, A. Pulvermuller, P. Trojan, J.H. Park, H.W. Choe, O.P. Ernst, K.P. Hofmann, U. Wolfrum, J. Biol. Chem. 279 (2004) 51472–51481.
[19] I.D. Acu, T. Liu, K. Suino-Powell, S.M. Mooney, A.B. D'Assoro, N. Rowland, A.R. Muotri, R.G. Correa, Y. Niu, R. Kumar, J.L. Salisbury, Cancer Res. 70 (2010) 3320–3328.
[20] R. Nishi, W. Sakai, D. Tone, F. Hanaoka, K. Sugasawa, Nucleic Acids Res. 41 (2013) 6917–6929.
[21] K. Sugasawa, DNA Repair 44 (2016) 110–117.
[22] X.J. He, J.Y. Feng, W. Wang, B.F. Chai, B.S. Yang, A.H. Liang, Acta Zool. Sin. 50 (2004) 447–451.
[23] L. Duan, Y.Q. Zhao, Z.J. Wang, G.T. Li, A.H. Liang, B.S. Yang, J. Inorg. Biochem. 102 (2008) 268–277.
[24] Y.Q. Zhao, L. Song, A.H. Liang, B.S. Yang, J. Photochem. Photobiol. B 95 (2009) 26–32.
[25] Y.Q. Zhao, X.J. Guo, B.S. Yang, RSC Adv. 7 (2017) 10206–10214.
[26] E.X. Shi, W.L. Zhang, Y.Q. Zhao, B.S. Yang, Metallomics 9 (2017) 1796–1808.
[27] Y.Q. Zhao, J.Y. Feng, A.H. Liang, B.S. Yang, Chin. Sci. Bull. 52 (2007) 3216–3220.
[28] Z.J. Wang, Y.Q. Zhao, L.X. Ren, G.T. Li, A.H. Liang, B.S. Yang, J. Photochem. Photobiol. A 186 (2007) 178–186.
[29] Y.Q. Zhao, J.Y. Feng, A.H. Liang, B.S. Yang, Spectrochim. Acta A 71 (2009) 1756–1761.
[30] Z.J. Rong, Y.Q. Zhao, E.X. Shi, W.L. Zhang, B.S. Yang, Electroanalysis 29 (2017) 1232–1242.
[31] W. Liu, L. Duan, T.J. Sun, B.S. Yang, Biometals 29 (2016) 1047–1058.
[32] Y.Q. Zhao, J. Yan, L. Song, Y.N. Feng, A.H. Liang, B.S. Yang, Spectrochim. Acta A 87 (2012) 163–170.
[33] L.X. Ren, Y.Q. Zhao, J.Y. Feng, X.J. He, A.H. Liang, B.S. Yang, Chinese J. Inorg. Chem. 22 (2006) 87–90.
[34] H. Hidaka, Y. Sasaki, T. Tanaka, T. Endo, S. Ohno, Y. Nagata, Proc. Natl. Acad. Sci. U. S. A. 78 (1981) 4354–4357.
[35] M. Osawa, M.B. Swindells, J. Tanikawa, T. Tanaka, T. Mase, T. Furuya, M. Ikura, J. Mol. Biol. 276 (1998) 165–176.
[36] D. Sasakura, W. Nunomura, Takakuwa, Biochem. Biophys. Res. Commun. 423 (2012) 360–365.
[37] M.D. Feldkamp, L. Gakhar, N. Pandey, M.A. Shea, Proteins 83 (2015) 989–996.
[38] J.R. Lakowicz, Kluwer Academic/Plenum, (1983), pp. 260–265.
[39] K. Arnold, L. Bordoli, J. Kopp, T. Schwede, Bioinformatics 22 (2006) 195–201.
[40] S.Y. Wu, M.D. Pérez, P. Puyol, L. Sawyer, J. Biol. Chem. 274 (1999) 170–174.
[41] Z. Song, W. Yuan, R.T. Zhu, S. Wang, C.F. Zhang, B.S. Yang, Int. J. Biol. Macromol. 96 (2016) 192–199.
[42] N.J. Greenfield, Nat. Protoc. 1 (2006) 2876–2890.
[43] M. Zhangh, T. Tanaka, M. Ikura, Nat. Struct. Mol. Biol. 2 (1995) 758–767.
[44] Z.J. Wang, L.X. Ren, Y.Q. Zhao, G.T. Li, L. Duan, A.H. Liang, B.S. Yang, Spectrochim. Acta, Part A 70 (2008) 892–897.
[45] P.D. Ross, S. Subramanian, Biochemistry 20 (1981) 3096–3102.
[46] M. Ishtikhar, S. Khan, G. Badr, A.O. Mohamed, R.H. Khan, Mol. BioSyst. 10 (2014) 2954–2964.
[47] G. Xiang, C. Tong, H. Lin, J. Fluoresc. 17 (2007) 512–521.
[48] M. Ishtikhar, E. Ahmad, Z. Siddiqui, S. Ahmad, M.V. Khan, M. Zaman, M.K. Siddiqi, S. Nusrat, T.I. Chandel, M.R. Ajmal, R.H. Khan, Int. J. Biol. Macromol. 107 (2018) 2450–2464.
[49] J. Martinez-Sanz, D. Grecu, L. Assairi, Bioenergetics 5 (2016) 236.